One Bipyridine and Triple Advantages:Tailoring Ancillary Ligand in Ruthenium complexes for Efficient Sensitization in Dye Solar Cells.

Chandrasekharam Malapaka,* Anil Reddy Marri, Surya Prakash Singh, B. Priyanka, Bhanuprakash Kotamarthi, Mannepalli Lakshmi Kantan, Islam Ashraful, Han Liyuan

Table of Contents:

General:

Sephadex LH-20 was procured from GE Healthcare Bio-Sciences AB, SE-75184, Uppsala and was used to purify the crude complexes on column chromatography. Dichloro (*p*-cymene) ruthenium (II) dimer, 2,2'-bipyridine-4,4'-dicarboxylic acid were prepared in accordance to the reported procedures. All solvents and reagents, unless otherwise stated, were of Laboratory Reagent Grade and used as received. Brucker 300 Avance ^{1}H NMR spectrometer run at 500 MHz was employed to record the NMR spectrum. Shimadzu LCMS-2010EV model with ESI probe was used to record mass spectra. Shimadzu UV-Vis spectrometer, model 1700 was used to record the electronic absorption spectrum of the ruthenium complexes. Emission measurements for these complexes were carried out in DMF using Fluorolog 3, J.Y.Horiba Fluorescence spectrometer. The electrochemical properties of ruthenium complexes were scrutinized by cyclic voltammetry using tetra-butyl ammonium perchlorate (0.1 M in acetonitrile) as a supporting electrolyte and ferrocene as an internal standard at 0.42 V *vs* SCE

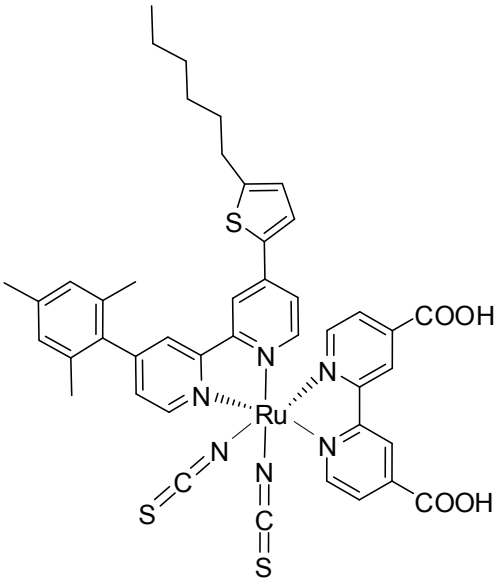

MC103

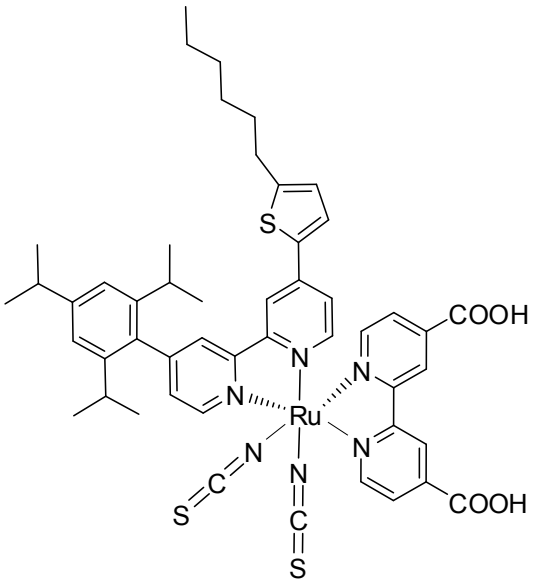

MC104

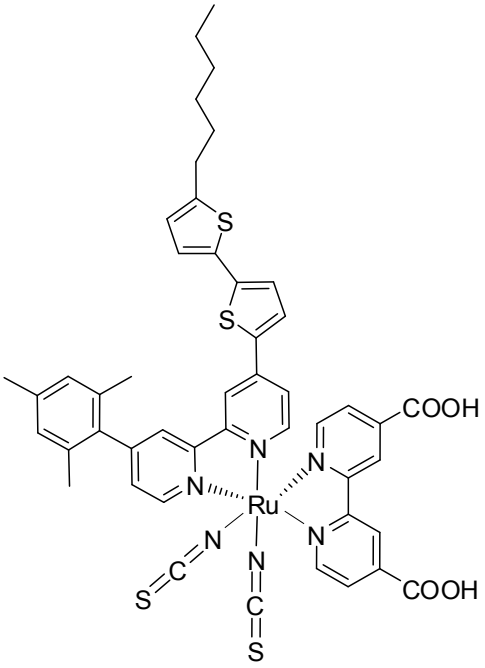

MC105

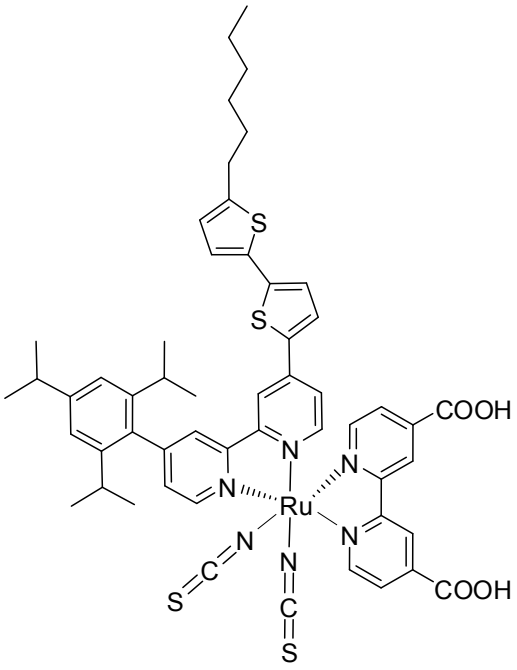

MC106

Figure S1. Structures of new sensitizers **MC**103-**MC**106.

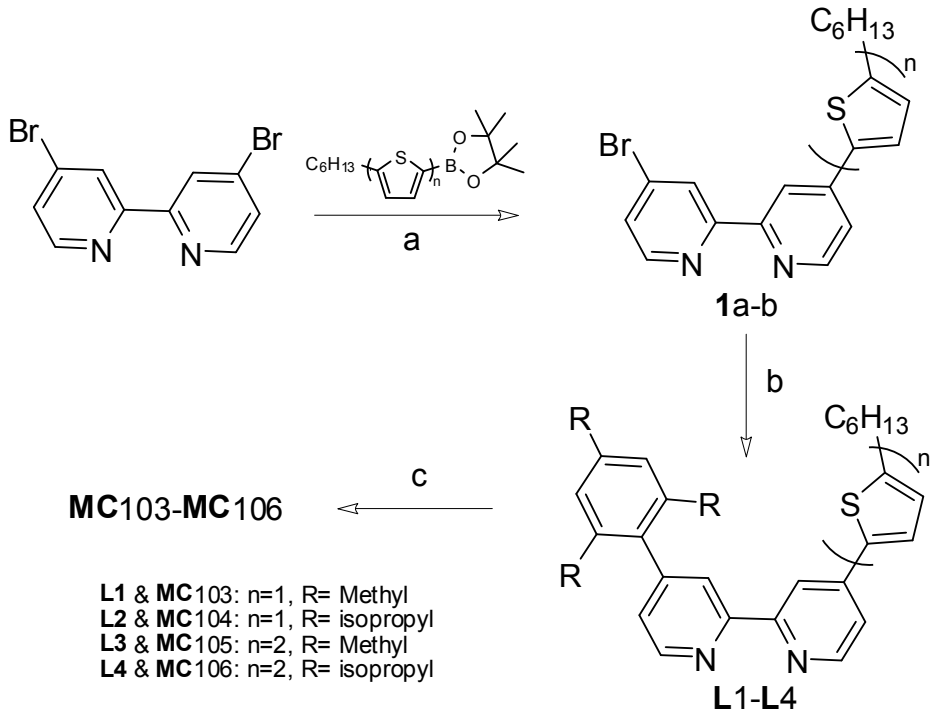

Scheme 1. Synthesis of sensitizers **MC**103-**MC**106. Reagents and conditions: a) $Pd(dppf)_2Cl_2$, KF, KOAc, DMF, 85^0 C; b) $ArB(OH)_2$, $Pd(PPh_3)_4$, 2M Na_2CO_3, DME, 90^0 C; c) $Ru(P\text{-cymene})_2Cl_2$, DMF, 60^0 C then Bipyridine dicarboxylic acid, NH_4SCN, 150^0 C.

General procedure for the synthesis of 4-substituted-4'-bromobipyridine

To a degassed solution of 4,4'-dibromobipyridine (500 mg, 1.592 mmol) in DMF (10 mL) were added the corresponding hexylthiophene boronic acid pinacol ester (1.592 mmol) dissolved in DMF (5 mL), $Pd(dppf)_2Cl_2$ (35 mg, 0.047 mmol), KOAc (1.56g, 15.92 mmol), KF (923 mg, 15.92 mmol) under argon atmosphere. The reaction mixture was heated at 85 ^{0}c for 7 h. The reaction mixture was filtered off and solvent was removed under reduced pressure. The crude compound was purified by silica gel column chromatography using hexane/ethyl acetate (9:1) to give 4-substituted-,4'-bromobipyridine.

4-bromo-4'-(5-hexylthiophen-2-yl)-2,2'-bipyridine (1a) (55%). ^{1}H NMR (300 MHz, $CDCl_3$, δ): 8.65 (s, 1H), 8.55-8.56 (m, 2H), 8.45-8.47 (d, 1H), 7.38-7.46 (m, 3H), 6.76-6.78 (d, 1H), 2.83 (t, 2H), 1.66-1.76 (m, 2H), 1.29-1.37 (m, 6h), 0.9 (t, 3H); ^{13}C NMR (300MHz, $CDCl_3$, δ) 157.54, 155.11, 149.73, 149.58, 148.80, 142.87, 133.91, 126.92, 125.61, 125.55, 124.60, 119.79, 116.94, 31.49, 30.34, 29.67, 28.7122.51, 14.05, **ESI-HRMS** calcd for $C_{20}H_{21}BrN_2S$ 401.0687, found 401.0691.

4-bromo-4'-(5'-hexyl-2, 2'-bithiophen-5-yl)-2,2'-bipyridine (1b):(55%). ^{1}H NMR (300 MHz, $CDCl_3$, □): 8.67 (s, 1H), 8.57-8.59 (d, 2H), 8.46-8.48 (d, 1H), 7.50-7.52 (d, 1H), 7.42-7.47 (m, 1H), 7.08-7.09 (d, 1H), 7.01-7.03 (d, 1H), 6.66-6.67 (d, 1H), 2.80 (t, 2H), 1.64-1.74 (m, 2H), 1.29-1.44 (m, 6h), 0.9 (t, 3H); 13C NMR (300MHz, $CDCl_3$, δ) 156.92, 155.87, 155.13, 149.78, 149.59, 146.56, 142.43, 140.19, 138.62, 134.02, 127.09, 126.60, 125.03, 124.71, 124.19, 123.96, 119.77, 116.97, 31.56, 30.22, 29.73, 28.77, 14.10. ESI-HRMS calcd for $C_{20}H_{21}BrN_2S$ 483.0564, found 483.0566.

General procedure for the synthesis of unsymmetrically substituted ancillary bipyridine ligand (L1-L4)

A 50 mL of Schlenk tube was charged with aryl boronic acid (1.0 mmol), $Pd(PPh_3)$ (115.4 mg, 0.1 mmol). Dimethoxy ethane(8 mL) and 2 M aqueous sodium carbonate (2 mL) were added, and the

tube was purged with argon gas with 5 evacuate /refill cycles. 4-substituted-,4'-bromobipyridine (1.0 mmol) was subsequently added as a neat liquid. The tube was sealed and heated at 90 ^{0}C vigorously for 18 h. Upon cooling to ambient temperature, the organics were extracted into dichloromethane (3 X 30 mL) from 30 mL water. The combined organics were washed with water (1 X 30 mL) and brine (1 X 30 mL), dried over Na_2SO_4, filtered and the solvent was removed under reduced pressure. The crude product was pre-adsorbed onto silica gel and chromatographed (9:1 hexane/ethyl acetate) to give unsymmetrically substituted bipyridine(L1-L4).

4-(5-hexylthiophene-2-yl)-4'-mesityl-2,2'-bipyridine (L1): ^{1}H NMR (300 MHz, $CDCl_3$, δ): 8.69-8.70 (d, 1H), 8.64 (s, 1H), 8.51-8.53 (d, 1H), 8.26 (s, 1H), 7.44-7.45 (d, 1H), 7.36-7.38 (d, 1H), 7.08-7.10 (d, 1H), 6.89 (s, 2H), 6.77-6.78 (s, 1H); FT-IR (KBr) (cm^{-1}): 2965, 2924, 2854, 1728, 1588, 1459, 1363, 1219, 1081, 974, 806, 721, 473. ^{13}C NMR (300MHz, $CDCl_3$, δ) 156.69, 156.28, 150.63, 149.70, 149.38, 148.57, 142.72, 138.65, 137.40, 136.47, 135.13, 128.26, 125.56, 125.50, 124.91, 122.27, 119.41, 116.86, 31.58, 30.40, 29.73, 28.77, 22.60, 21.09, 20.68, 14.11. ESI-HRMS calcd for $C_{29}H_{32}N_2S$ 441.2364, found 441.2364.

4-(5-hexylthiophene-2-yl)-4'-triisopropylphenyl-2,2'-bipyridine (L2): ^{1}H NMR (300 MHz, $CDCl_3$, δ): 8.68-8.69 (d, 1H), 8.65 (s, 1H), 8.49-8.51 (d, 1H), 8.33 (s, 1H), 7.44-7.45 (d, 1H), 7.35-7.38 (d, 1H), 7.11-7.14 (d, 1H), 7.01 (s, 2H), 6.78-6.79 (d, 1H), 2.82-2.96 (m, 3H), 2.52-2.62 (m, 2H), 1.68-1.78 (m, 2H), 1.09-1.41 (m, 24H), 0.91 (t, 3H); ^{13}C NMR (300MHz, $CDCl_3$, δ) 156.51, 155.66, 150.49, 149.70, 148.74, 148.66, 148.45, 145.71, 142.57, 138.59, 134.57, 125.47, 125.38, 125.29, 122.76, 120.64, 120.14, 119.30, 116.80, 34.84, 34.29, 31.85, 31.49, 30.31, 29.64, 28.68, 24.61, 24.20, 24.05, 22.51, 14.02. FT-IR (KBr) (cm^{-1}): 2959, 2927, 2856, 1588, 1466, 1365, 1104, 1057, 803, 721, 492.ESI-HRMS calcd for $C_{35}H_{44}N_2S$ 525.3303, found 525.3318.

4-(5'-hexyl-2,2'-bithiophen-5-yl)-4'-mesityl-2,2'-bipyridine (L3):^{1}H NMR (300 MHz, $CDCl_3$, δ): 8.70-8.71 (d, 1H), 8.68 (s, 1H), 8.54-8.55 (d, 1H), 8.28 (s, 1H), 7.53-7.54 (d, 1H), 7.39-7.40 (d, 1H), 7.10 (s, 1H), 7.02-7.03 (d, 1H), 6.89 (s, 2H), 6.67 (d, 1H), 2.80 (t, 3H), 2.32 (s, 3H), 2.04 (s, 6H), 1.66-1.72 (m, 2H), 1.33-1.44 (m, 6H), 0.91 (t, 3H); 13C NMR (300MHz, $CDCl_3$, δ) 156.80, 156.13, 150.69, 149.78, 149.41, 146.42, 142.14, 139.87, 139.08, 137.40, 136.44, 135.13, 134.23, 128.29, 126.37, 125.03, 124.10, 123.96, 122.30, 119.33, 116.83, 31.59, 30.22, 29.73, 28.76, 22.60, 21.09, 20.68, 14.13.FT-IR (KBr) (cm^{-1}): 2961, 2924, 2854, 1590, 1452, 1363, 1202, 1041, 840, 797, 725, 476.ESI-HRMS calcd for $C_{33}H_{34}N_2S_2$ 523.2241, found 523.2231.

4-(5'-hexyl-2, 2'-bithiophen-5-yl)-4'-triisopropylphenyl-2,2'-bipyridine (L4):^{1}H NMR (300 MHz, $CDCl_3$, δ): 8.69-8.71 (m, 1H), 8.52-8.54 (d, 1H), 8.35 (s, 1H), 7.54-7.55 (d, 1H), 7.39-7.41 (d, 1H), 7.13-7.15 (d, 1H), 7.09-7.11 (d, 1H), 7.02-7.03 (m, 3H), 6.66-6.68 (d, 1H), 2.78-2.96 (m, 3H), 2.52-2.62 (m, 2H), 1.64-1.74 (m, 2H), 1.09-1.34 (m, 24H), 0.91 (t, 3H); 13C NMR (300MHz, $CDCl_3$, δ) 156.74, 155.64, 150.63, 148.86, 148.77, 146.42, 145.83, 142.08, 139.81, 139.11, 134.63, 126.34, 125.47, 125.03, 124.07, 123.96, 122.88, 120.73, 119.30, 116.86, 34.96, 34.38, 31.59, 30.43, 30.22, 29.73, 28.77, 24.69, 24.28, 24.13, 22.60, 14.13.FT-IR (KBr) (cm^{-1}): 2960, 2921, 2873, 1589, 1459, 1363, 1065, 876, 794, 719, 481.ESI-MS calcd for $C_{39}H_{46}N_2S_2$ 607.3180, found 607.3000

General procedure for the synthesis of ruthenium complex (MC103-MC106)

A solution of ligand **L1** (200 mg, 0.454 mmol) and dichloro(p-cymene)-ruthenium dimmer (139 mg, 0.227 mmol) dissolved in dry DMF (200 mL) was heated at 60 ^{0}C for 4 h under nitrogen atmosphere in the dark. Subsequently, 4,4'-dicarboxyllic acid-2,2'-bipyridine (111 mg, 0.454 mmol) was added and the reaction mixture was heated to 140 ^{0}C for another 4 h. To the resulting dark green solution was added solid NH_4NCS (1.038g, 13.635 mmol) and the reaction mixture was further heated for 4 h at 140 ^{0}C. After completion of the reaction (monitored by absorption) the reaction mixture was cooled to room temperature and the solvent was removed under reduced pressure and water (200 mL) was added to get precipitate. The purple solid was filtered off and washed with distilled water, ether and dried under vacuum. The crude compound was dissolved in

methanol and further purified on sephadex LH-20 methanol as eluent. The main band was collected and concentrated to give

MC103 (65%). ^{1}H NMR (300 MHz, $CDCl_3$+CD_3OD, δ): 9.73-9.76 (s, 1H), 9.36-9.55 (dd, 1H), 8.94 (s, 1H), 8.82 (d, 1H), 7.77-8.28 (m, 4H), 7.61-7.68 (m, 2H), 7.37-7.47 (dd, 1H), 7.28-7.30 (d, 1H), 7.16-7.19 (d, 1H), 7.11 (s, 1H), 6.81-7.00 (m, 3H), 2.80-2.95 (tt, 2H), 2.33-2.42 (d, 3H), 2.21 (s, 3H), 1.86-2.05 (d, 3H), 1.65-1.69 (m, 2H), 1.30-1.45 (m, 6H), 0.84-0.93 (m, 3H).FT-IR (KBr) (cm-1): 2954, 2925, 2854, 2101(N=C), 1720(C=O), 1609, 1544, 1461, 1409, 1376, 1309, 1257, 1231, 1019, 900, 849, 808, 770, 661.

MC104 (62%). ^{1}H NMR (300 MHz, $CDCl_3$+CD_3OD, δ): 9.74-9.77 (s, 1H), 9.37-9.54 (dd, 1H), 8.94-8.96 (s, 1H), 8.80-8.83 (d, 1H), 7.88-8.29 (m, 4H), 7.61-7.74 (m, 3H), 7.32-7.38 (dd, 1H), 6.80-7.24 (m, 4H), 2.68-3.05 (m, 5H), 1.64-1.68 (m, 2H), 1.05-1.43 (m, 24H), 0.86-0.93 (m, 3H).180.FT-IR (KBr) (cm^{-1}): 2957, 2923, 2859, 2101(N=C), 1720(C=O), 1607,1537, 1459, 1410, 1372, 1310, 1259, 1226, 1063, 1020, 891, 805, 664.

MC105 (63%). ^{1}H NMR (300 MHz, $CDCl_3$+CD_3OD, δ): 9.73-9.76 (s, 1H), 9.38-9.55 (dd, 1H), 8.95 (s, 1H), 8.81-8.82 (d, 1H), 8.07-8.33 (m, 3H), 7.49-7.94 (m, 4H), 6.96-7.34 (m, 6H), 6.71-6.78 (d, 1H), 2.77-2.86 (m, 2H), 2.34-2.42 (d, 3H), 2.22 (s, 3H), 1.87-2.05 (d, 3H), 1.65-1.74 (m, 2H),1.32-1.43 (m, 6H), 0.86-0.91 (m, 3H). FT-IR (KBr) (cm^{-1}): 3062, 2920, 2853, 2098(N=C), 1715(C=O), 1605, 1535, 1469, 1437, 1408, 1374, 1307, 1259, 1226, 1128, 1019, 898, 847, 798, 665, 571.

MC106 (65%). ^{1}H NMR (300 MHz, $CDCl_3$+CD_3OD, δ): 9.73-9.75 (s, 1H), 9.38-9.54 (dd, 1H), 8.98 (s, 1H), 8.84-8.85 (d, 1H), 8.15-8.37 (m, 3H), 7.91-7.98 (dd, 1H), 7.67-7.79 (m, 3H), 7.37-7.50 (dd, 1H), 7.23-7.24 (s, 2H), 6.98-7.17 (m, 3H), 6.71-6.77 (d, 1H), 2.71-3.08 (m, 5H), 1.62-1.77 (m, 2H), 1.06-1.38 (m, 24H), 0.88-0.93 (m, 3H).**FT-IR** (KBr) (cm^{-1}): 3066, 2957, 2923, 2861, 2099(N=C), 1720(C=O), 1608, 1538, 1466, 1410, 1373, 1312, 1230, 1118, 1065, 1021, 802, 667.

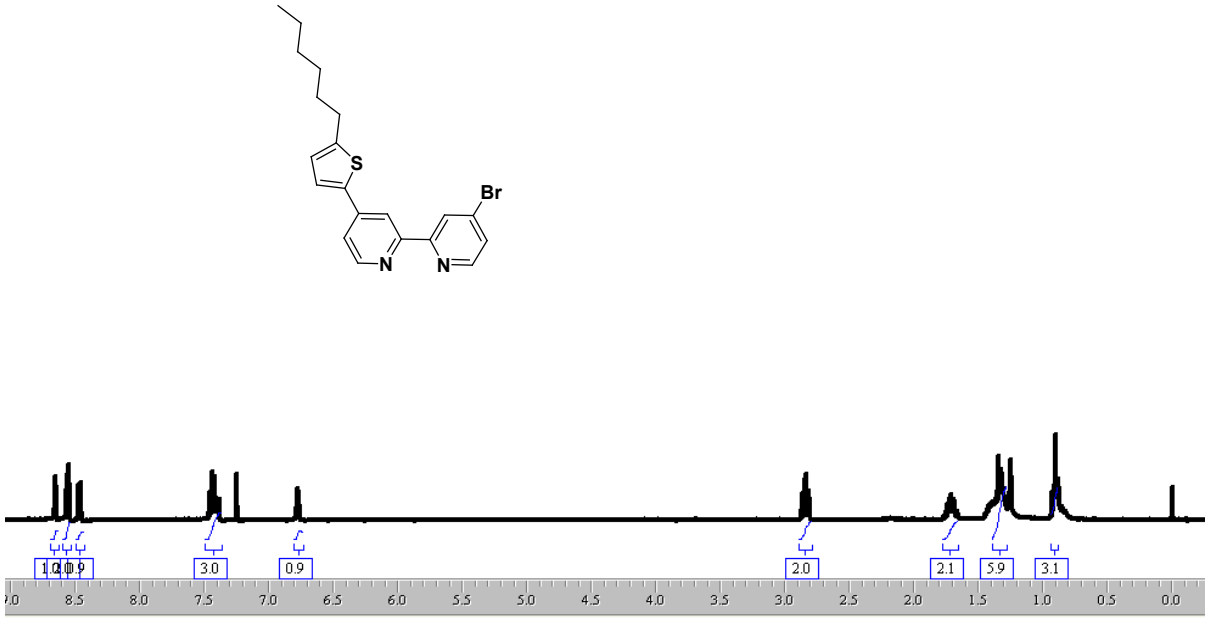

Figure S2. 1HNMR of 4-bromo-4'-(5-hexylthiophen-2-yl)-2,2'-bipyridine (1a).

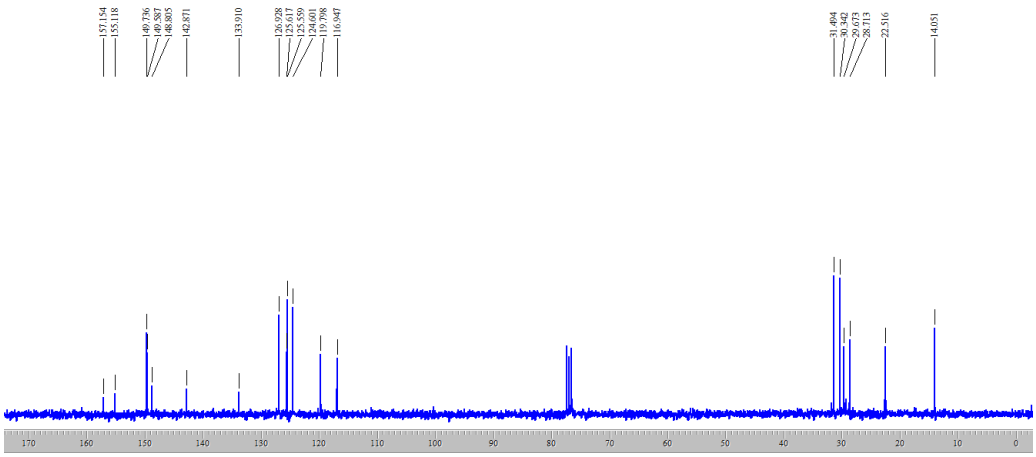

Figure S3. 13CNMR of 4-bromo-4'-(5-hexylthiophen-2-yl)-2,2'-bipyridine (1a).

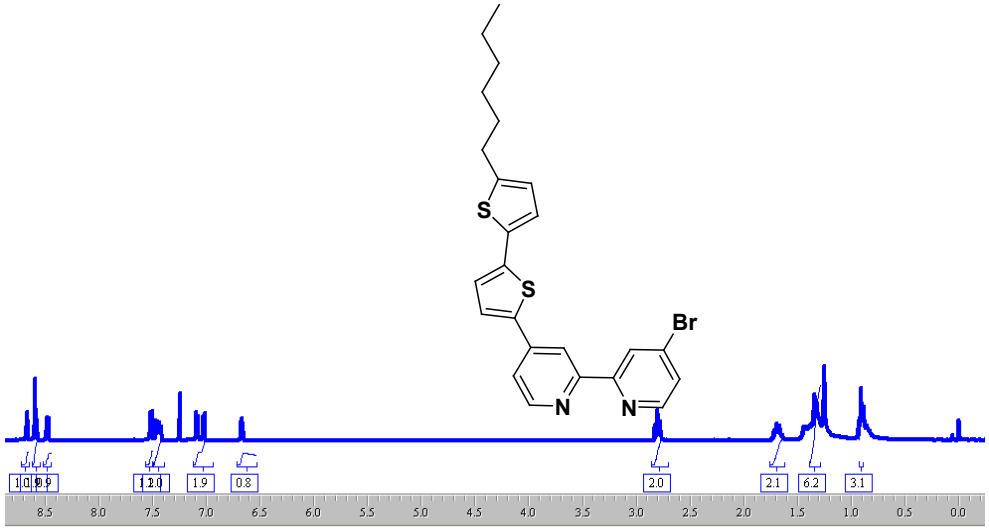

Figure S4. 1HNMR of 4-bromo-4'-(5'-hexyl-2, 2'-bithiophen-5-yl)-2,2'-bipyridine (1b).

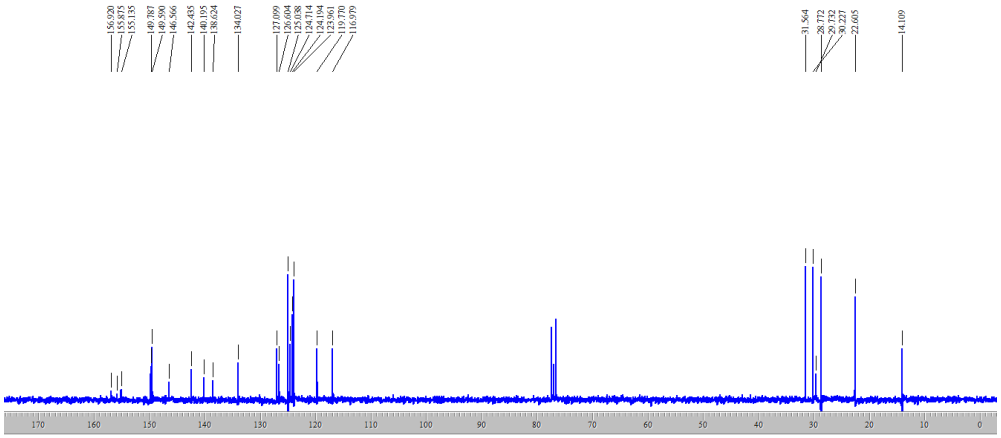

Figure S5. 13CNMR of 4-bromo-4'-(5'-hexyl-2, 2'-bithiophen-5-yl)-2,2'-bipyridine (1b).

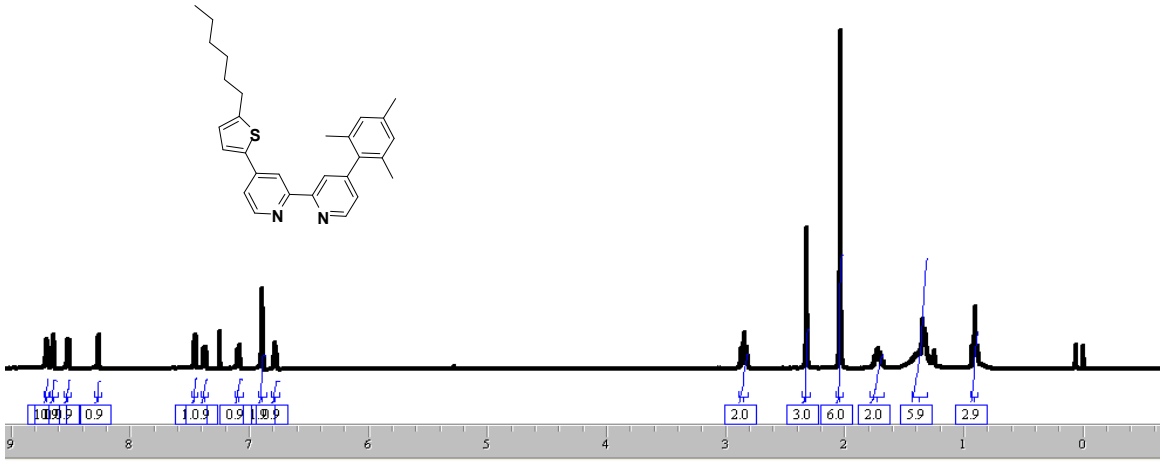

Figure S6. 1HNMR of **L**1.

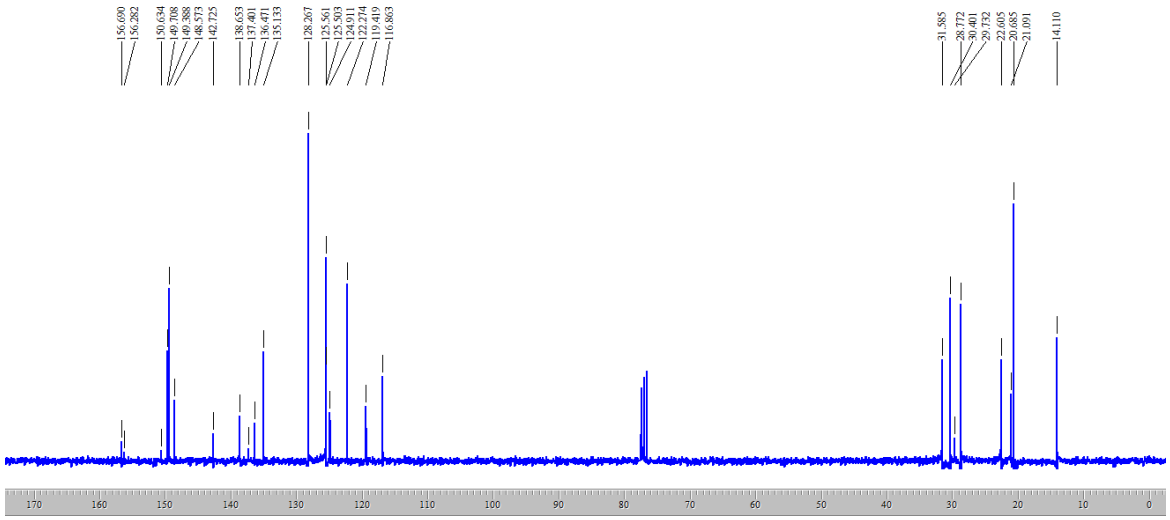

Figure S7. 13CNMR of **L**1.

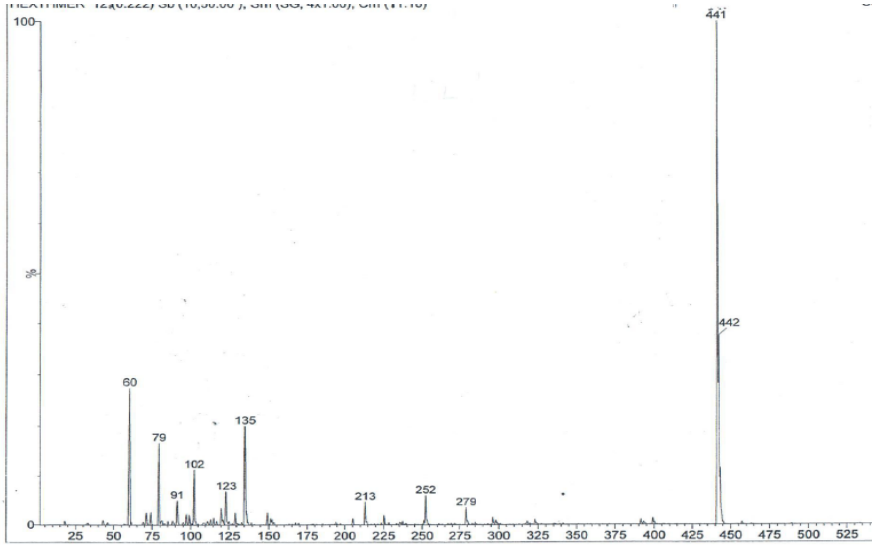

Figure S8. Mass Spectrum of **L**1.

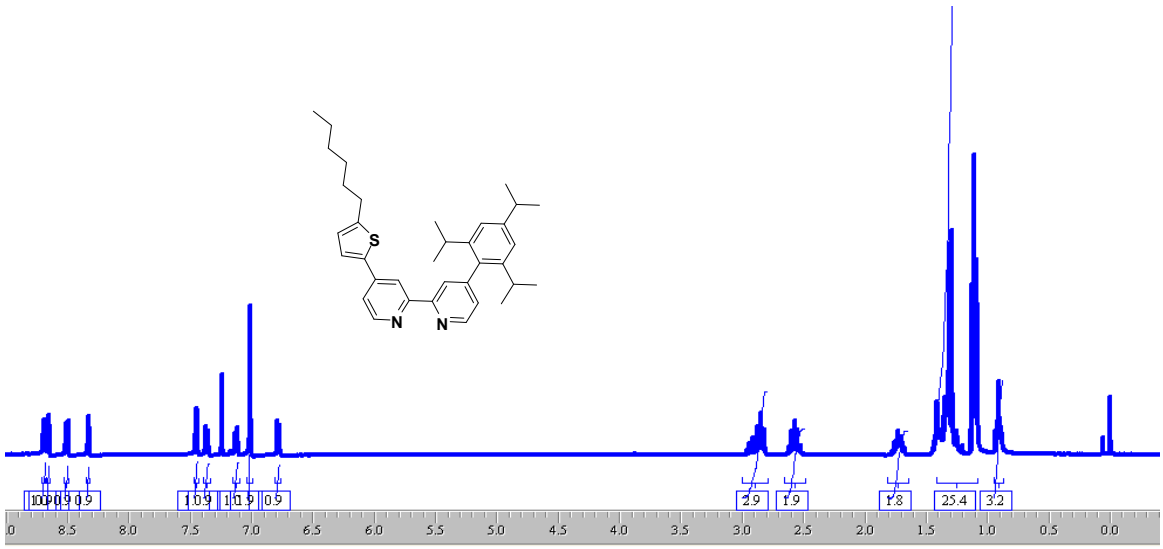

Figure S9. 1HNMR of **L**2.

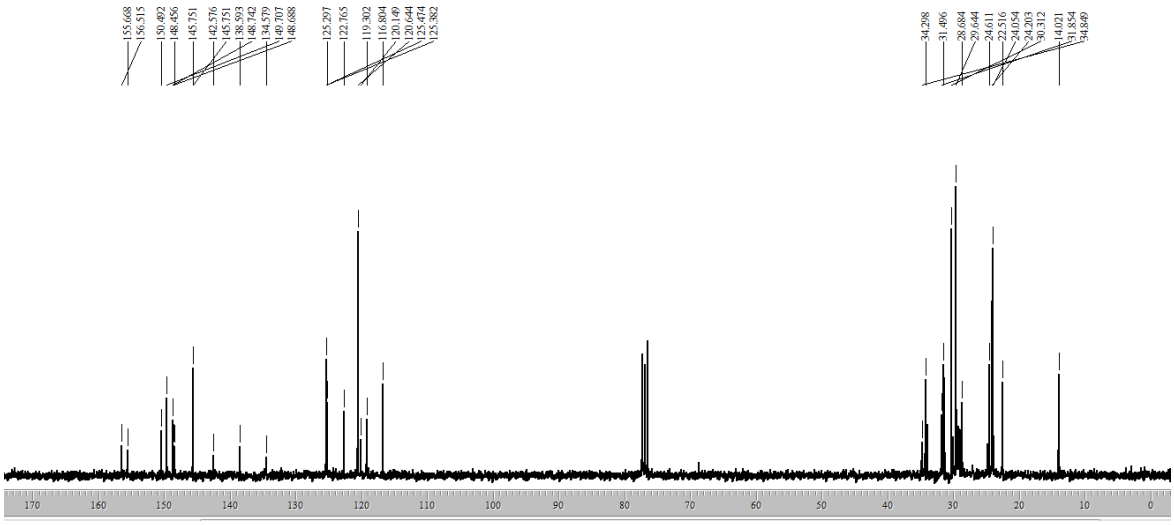

Figure S10. 13CNMR of **L**2.

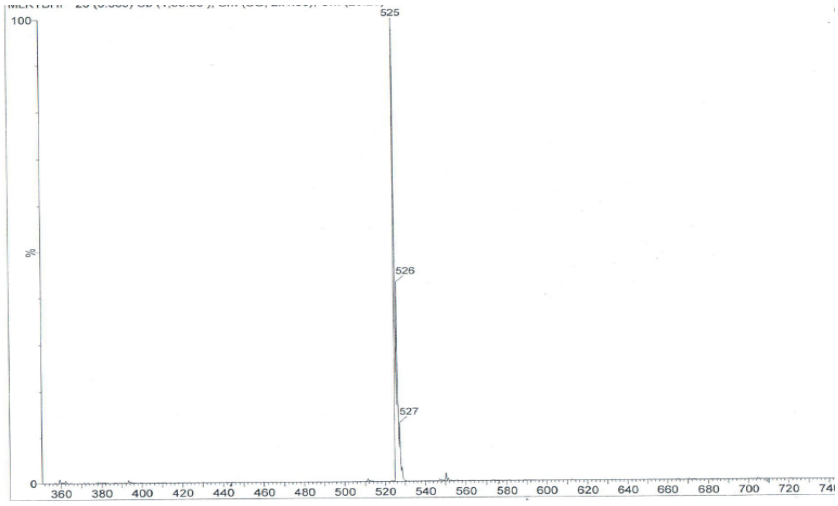

Figure S11. Mass Spectrum of **L**2.

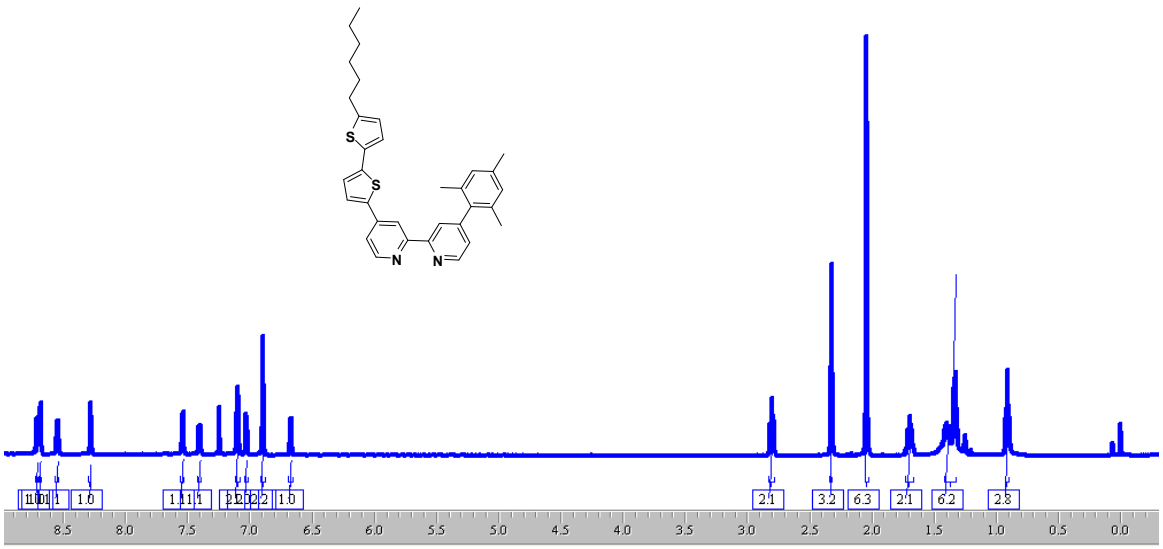

Figure S12. 1HNMR of **L**3.

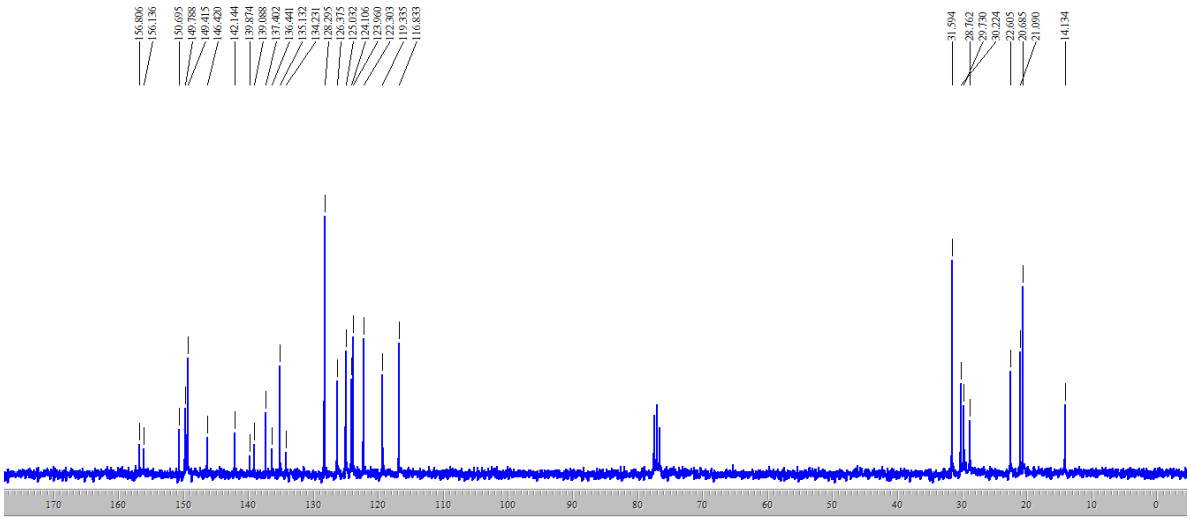

Figure S13. 13CNMR of **L**3.

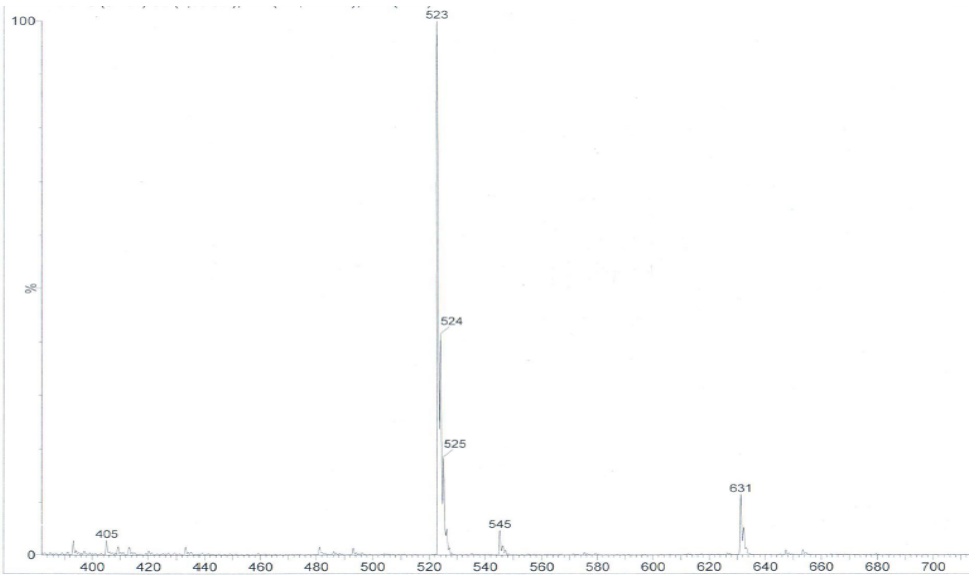

Figure S14. Mass Spectrum of **L**3.

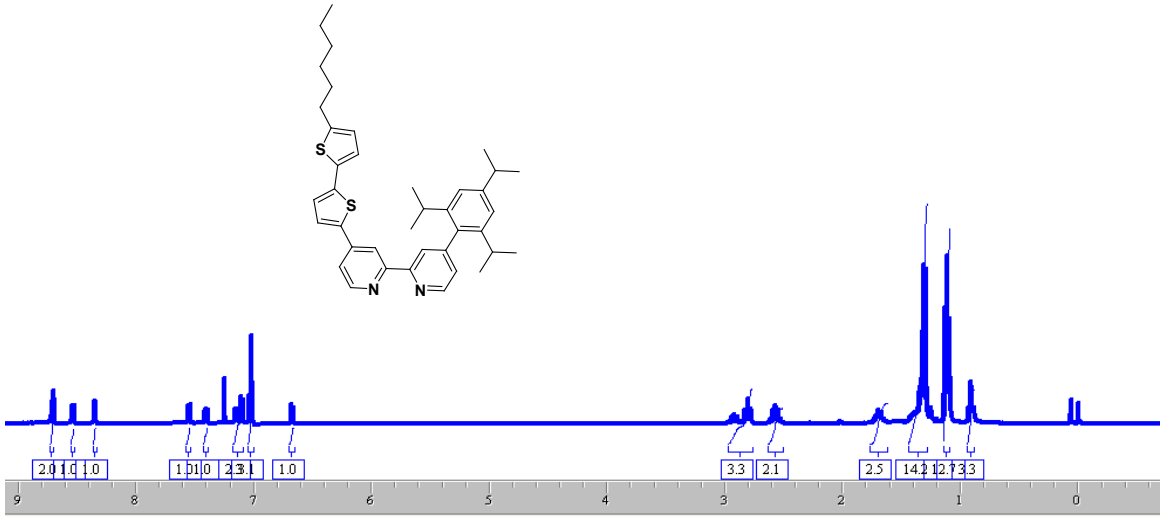

Figure S15. 1HNMR of **L**4.

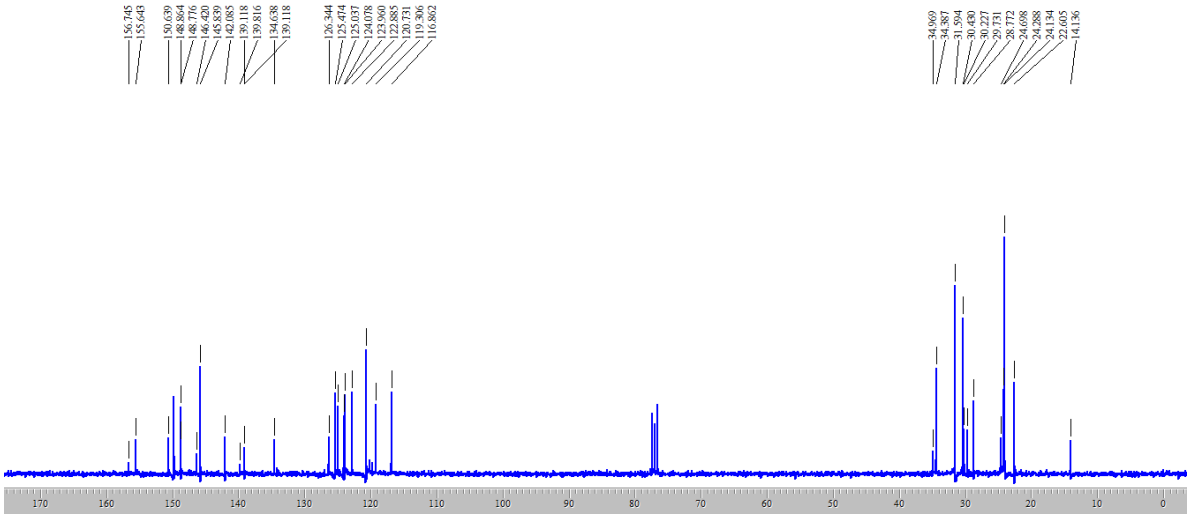

Figure S16. 13CNMR of **L**4.

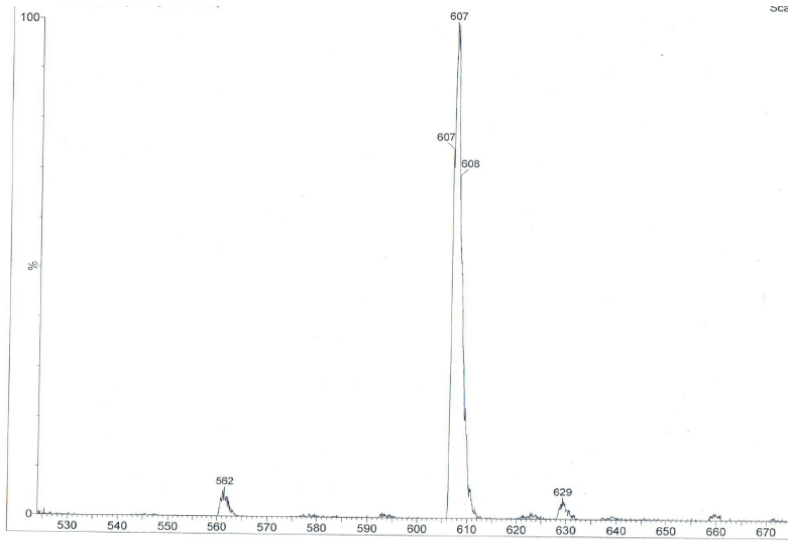

Figure S17. Mass Spectrum of **L**4.

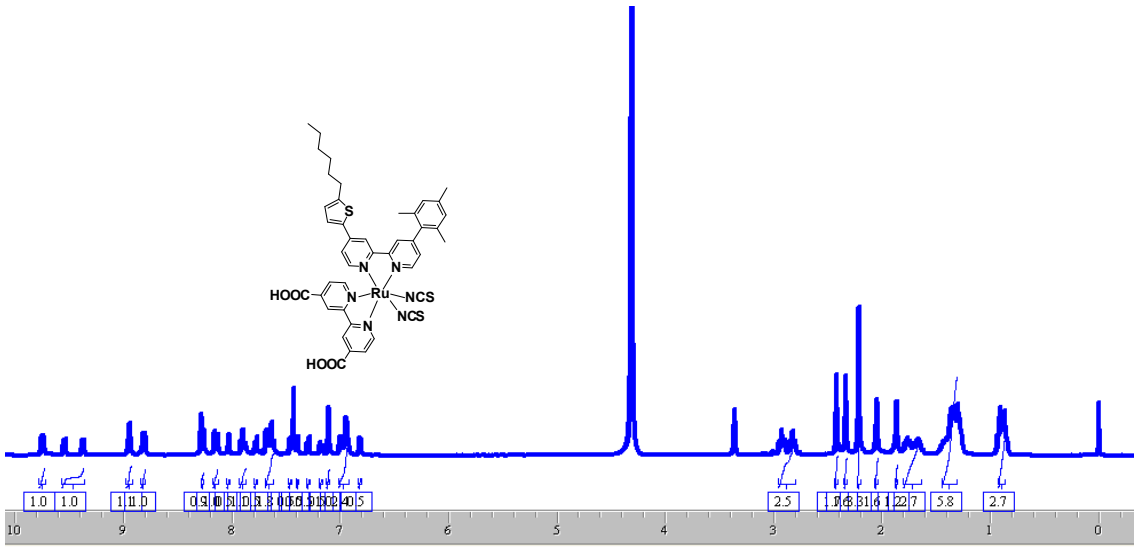

Figure S18. 1HNMR of **MC**103.

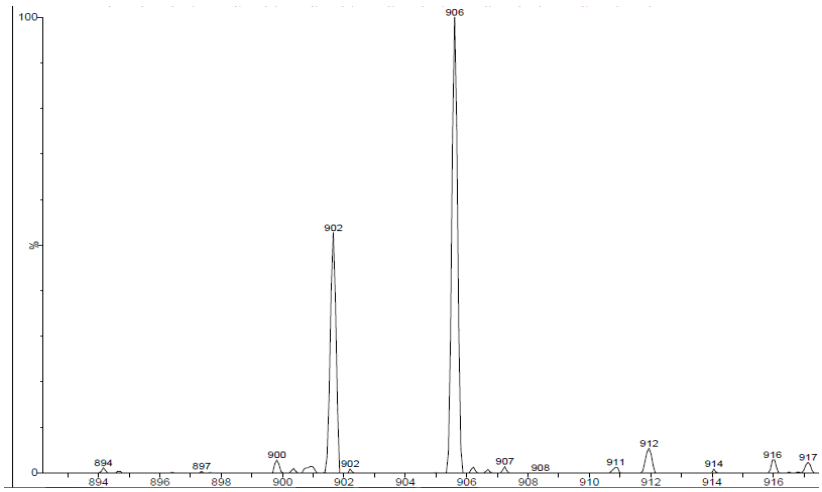

Figure S19. Mass Spectrum of **MC**103.

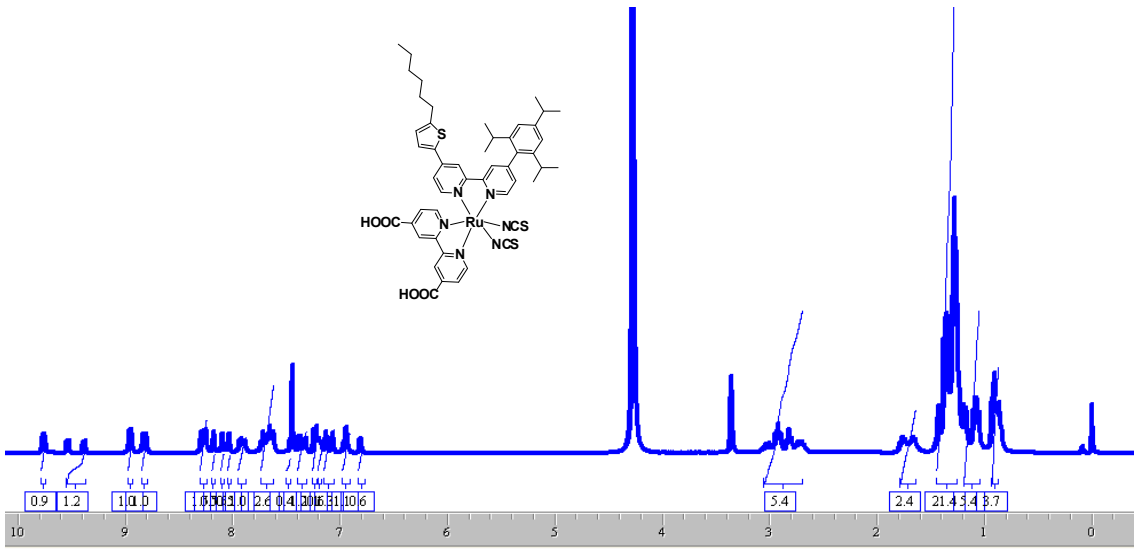

Figure S20. 1HNMR of **MC**104.

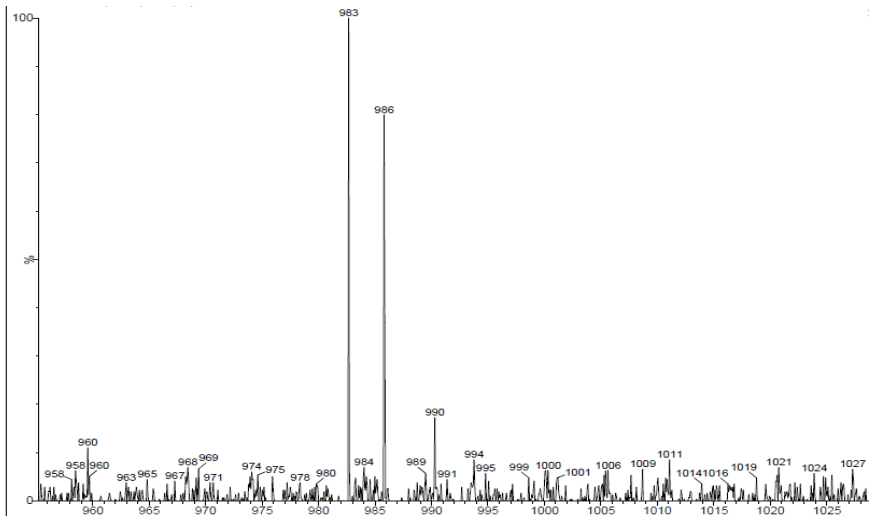

Figure S21. Mass Spectrum of **MC**104.

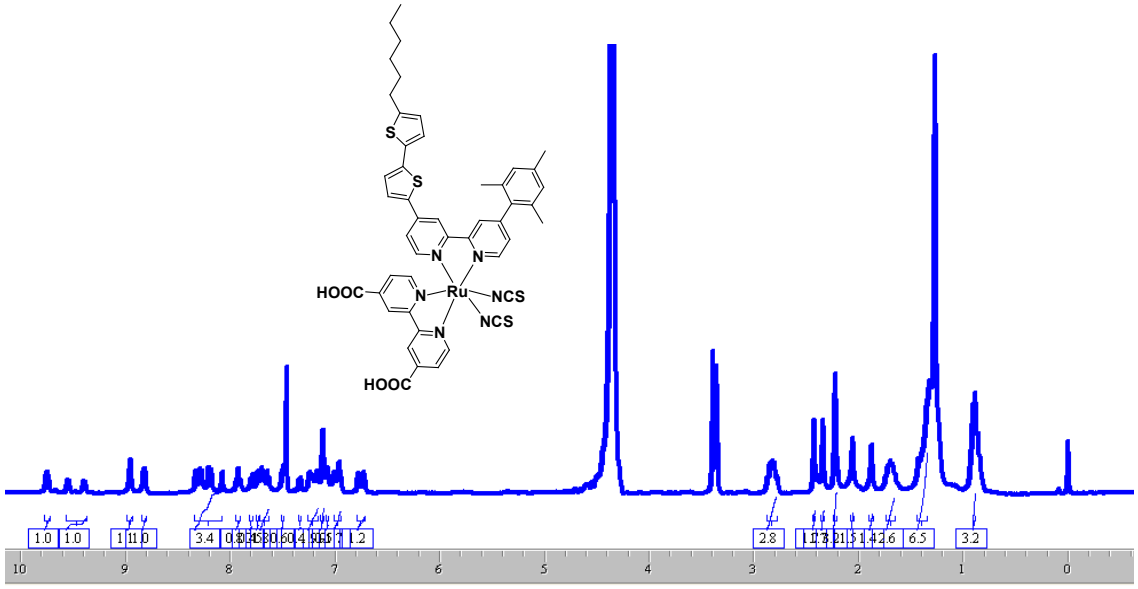

Figure S22. 1HNMR of **MC**105.

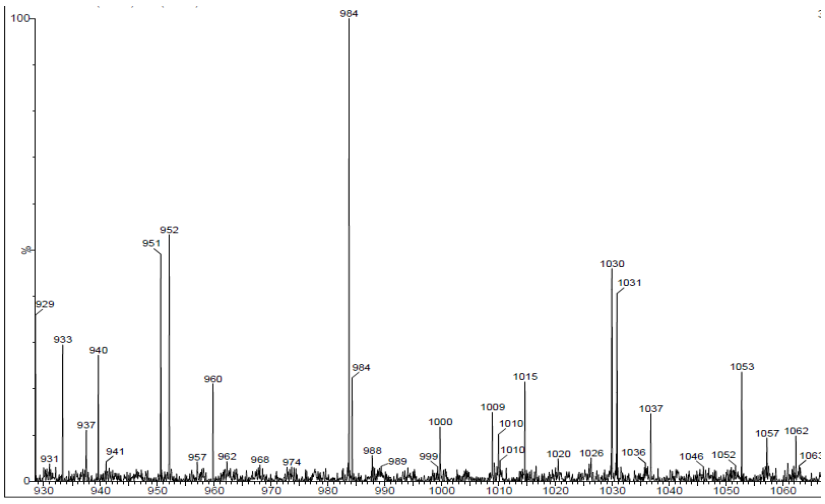

Figure S23. Mass Spectrum of **MC**105.

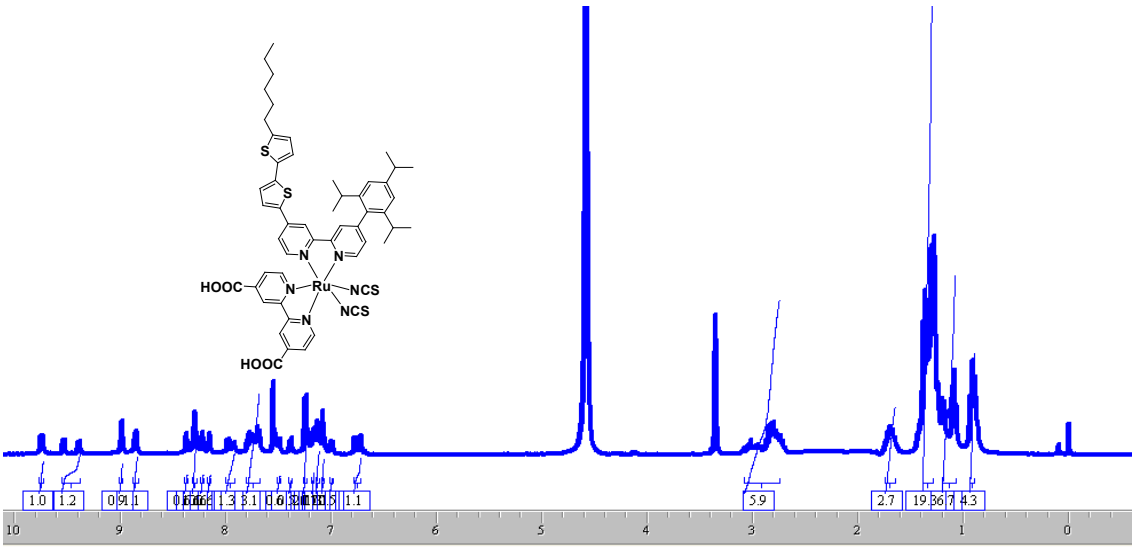

Figure S24. 1HNMR of **MC**106.

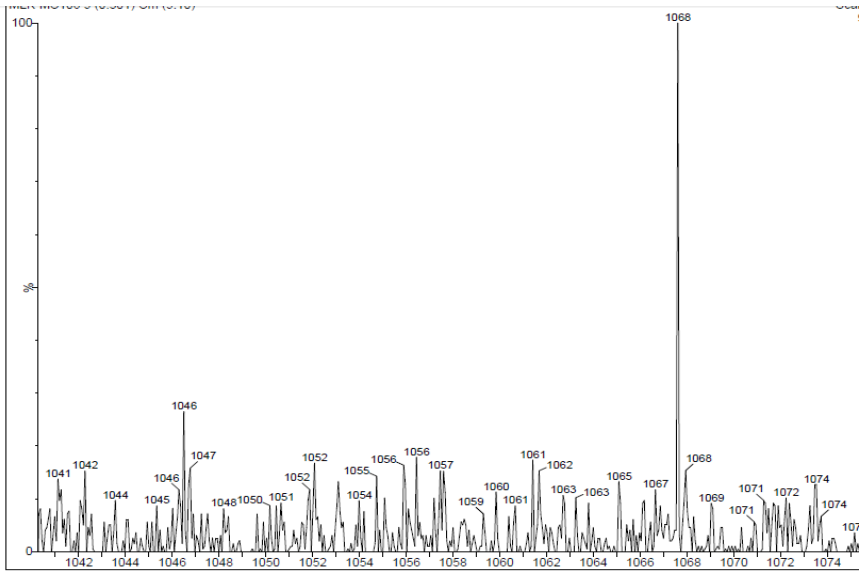

Figure S25. Mass Spectrum of **MC**106.

Fabrication of the device and Measurements.

The state-of-the art mesoporous titania film composed of 10 µm thickness layer of 13 nm sized TiO_2 particles followed by a second layer of 4 µm thickness with 200 nm size particles were screen printed (area: 0.25 cm^2) over a fluorine-doped SnO_2 (FTO) conducting glass. The dye solutions (2 x 10^{-4} M) were prepared in 1:1 acetonitrile and tert-butyl alcohol solvents and Deoxycholic acid as a co-adsorbent was added at a concentration of 20 mM. The TiO_2 surface was derivatised by immersing the electrodes in the dye solutions and then kept at 25 ^{0}C for 20 h. The dye deposited TiO_2 film and a platinum-coated conducting glass were separated by a Surlyn spacer (40 mm thick) and sealed by heating the polymer frame. The current–voltage characteristics were measured using a black metal mask with an aperture area of 0.231 cm^2 under standard air mass 1.5 sunlight (100 $mWcm^{-2}$, WXS-155S-10: Wacom Denso Co. Japan). Monochromatic incident photon-to-current conversion efficiency spectra were measured with a monochromatic incident light of $1x10^{16}$ photons cm^{-2} in director current mode (CEP-2000BX,Bunko-Keiki).

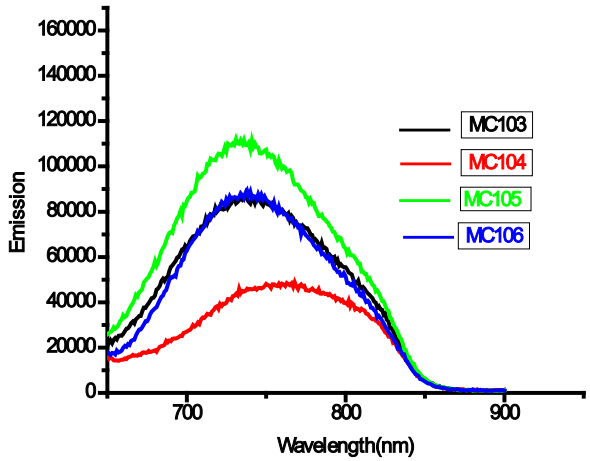

Figure S26. Emission spectra of the sensitizers **MC**103- **MC**106.

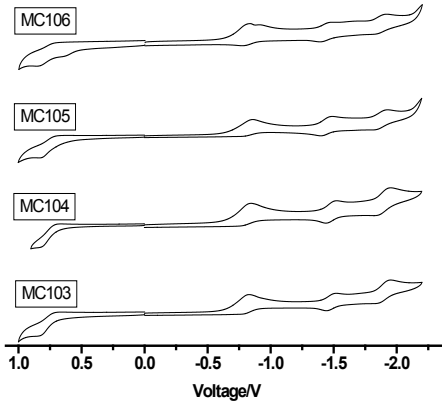

Figure S27. Cyclic voltammograms for the sensitizers **MC**103- **MC**106.

Table 1: Absorption, emision, electrochemical data of the sensitizers **MC**103-**MC**106.

Dye	λ_{max}(ε X $M^{-1}cm^{-1}$) [nm][a]	λ_{em} [nm][a]	E_{red}/ (1^{st}) [V][b]	E_{red}/(2^{nd}) [V][b]	E_{red}/(3^{rd}) [V][b]	E_{ox}/(1^{st}) [V][b]	$E_{0\text{-}0}$ [eV][c]
MC103	533 (1.625)	740	0.814	1.477	1.902	0.770	1.898
MC104	532 (1.380)	762	0.824	1.484	1.898	0.758	1.890
MC105	546 (2.015)	734	0.833	1.446	1.882	0.763	1.893
MC106	545 (1.789)	740	0.807	1.430	1.875	0.682	1.931

[a] Absorption and Emission spectra were recorded in DMF solutions at 298K. [b] Redox potetials were measured by cyclic-voltammetry. [c] The bandgap, $E_{0\text{-}0}$, was derived from the intersection of the absorption and emission spectra.

Computational Details:

Gaussian 09 was employed for all the calculations. The ground state geometry of complex **MC**103 and **MC**105 was optimized by hybrid functional Becke Three Parameter B3LYP with Los Alamos electron effective core potential. LANL2DZ basis set was selected for our study.

In order to reduce the computational cost we have replaced the hexyl group of the ancillary Ligand(L_A) with methyl group, as alkyl chain hardly have any influence in spectral properties. In the calculation the quasi-relativistic pseudo-potentials proposed by Hay and Wadt and a double zeta quality basis set LANL2DZ was adopted on all the atoms.

At the optimized geometry TDDFT calculations were performed at same level of theory in DMF by means of PCM solvation model as implemented in the Gaussian 09 program package. 70 singlet-singlet excitations at the S0 optimized geometry allowed us to simulate a large (upto 300 nm) portion of the absorption spectrum and gain insight into the nature of the transitions giving rise to the low energy spectral region.

TD-DFT calculations:

TDDFT calculations were employed to better understand the nature of the excited states and examine the vertical excitation energies. TDDFT calculations in the framework of the PCM model DMF solvent gives very good agreement with experimental one, shows their respective simulated spectra,

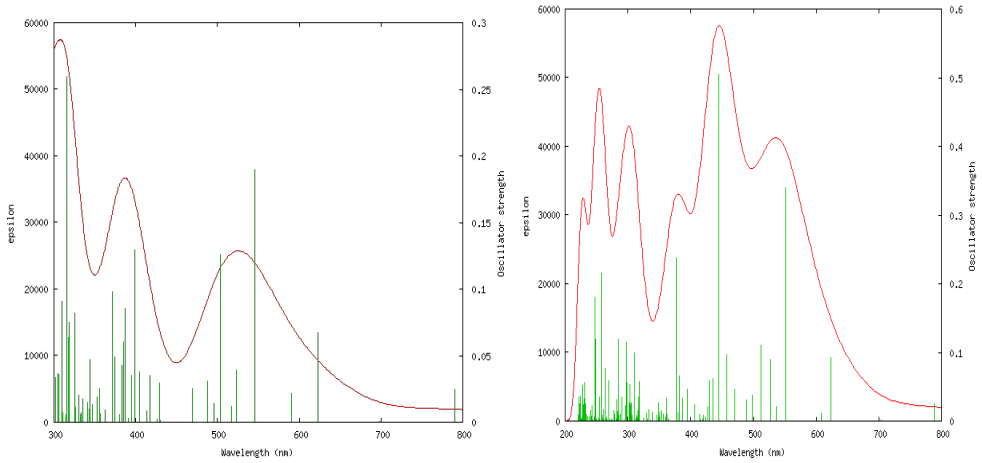

Figure S28. Simulated UV-Vis absorption spectra for MC103 and MC105 at B3LYP/LANL2DZ level in solvent (DMF) phase.

Calculated first 10 singlet excited states along with their energies and oscillator strength are given in Table 2 & Table 3.
A closer look at the TDDFT eigen vectors helps in assigning the main spectral feature in terms of their singly occupied to virtual molecular orbital contributions. Calculated λ_{max} peak for the MC103 and MC105 is at 546nm 552nm respectively well in agreement with the experimental values. These transitions mainly takes from homo energy level to lowest unoccupied suggesting these are mixture of LLCT and MLCT.

***Table 2*:** Singlet excited states calculated at the B3LYP/LANL2DZ level using PCM solvation model for MC103

States	Participating MO	E(eV)	λ(nm)	f
S1	Homo->Lumo	1.5695	789.95	0.0244
S2	Homo-1->Lumo	1.7767	697.83	0.0008
S3	Homo-2->Lumo	1.9897	623.14	0.0668
S4	Homo->Lumo+2	2.0991	590.65	0.0217
S5	Homo->Lumo+1	2.2718	545.75	0.1897
S6	Homo-1->Lumo+1	2.3712	522.86	0.0389
S7	Homo-1->Lumo+1	2.3971	517.22	0.0121
S8	Homo-2->Lumo+2	2.4638	503.23	0.1259
S9	Homo-2->Lumo+1 Homo-1->Lumo+2	2.4996	496.02	0.0140
S10	Homo-3->Lumo	2.5407	488.00	0.0311

Table 3: Singlet excited states calculated at the B3LYP/LANL2DZ level using PCM solvation model for MC105

States	Participating MO	E(eV)	λ(nm)	f
S1	Homo->Lumo	1.5721	788.65	0.0248
S2	Homo-1->Lumo	1.7617	703.79	0.0011
S3	Homo-2->Lumo	1.9886	623.46	0.0928
S4	Homo->Lumo+1	2.0357	609.04	0.0109
S5	Homo->Lumo+2	2.2467	551.85	0.3403
S6	Homo- 2->Lumo+2	2.3130	536.04	0.0214
S7	Homo-1->Lumo+2 Homo-1->L+2	2.3537	526.77	0.0891
S8	Homo-1->Lumo+2	2.4189	512.56	0.1107
S9	Homo-3->Lumo	2.4584	504.32	0.0003
S10	Homo-2->Lumo+2	2.4868	498.56	0.0378

To gain insight into the electronic structure of complexes we report in Table 4 & Table 5 the important molecular orbital composition and in figure S29 & figure S30 the isodensity surface plots of some selected molecular orbitals. The calculations show that for both the molecules HOMO is centered on Ru-d orbitals and the NCS ligand wheras LUMO is a π^* orbital centered mainly on the cyclometalating ligand(dcbpy). H – 1, H - 2 is centered on NCS ligand .Wheras L+1 is centered mainly on the ancillary Ligand(L_A) and also on dcbpy, L+2 is composed of mainly dcbpy and to some extent on L_A for **MC**103 .As in the case of **MC**105 ancillary ligand has main contribution on L+1 and dcbpy on L+2. In short the major contribution for highest occupied orbitals are composed of NCS ligand and Ru(d) orbitals. For the lowest unoccupied have both dcbpy and L_A compositions.

Table 4: Molecular orbital composition (%) in the ground state at the B3LYP/LANL2DZ level for **MC**103

Orbital	Energy(eV)	Ru	Ru(d)	NCS	dcbpy	L_A	Main bond Nature
Homo-5	-6.344	61.0	60.6	19.4	8.3	11.4	Ru(d)+NCS
Homo-4	-6.255	51.8	51.5	11.6	8.9	27.8	Ru(d)+ L_A
Homo-3	-5.071	1.8	1.4	92.0	1.9	4.4	NCS
Homo-2	-4.977	16.0	15.9	75.8	4.0	4.2	NCS
Homo-1	-4.893	12.6	12.3	77.8	6.1	3.5	NCS
Homo	-4.754	21.3	21.0	66.8	7.5	4.4	NCS+Ru(d)
Lumo	-3.245	10.8	10.8	2.5	83.2	3.4	dcbpy
Lumo+1	-2.895	3.8	3.7	0.8	21.0	74.5	L_A+dcbpy
Lumo+2	-2.798	4.7	4.6	0.7	76.3	18.3	dcbpy
Lumo+3	-2.375	0.4	0.2	0.1	85.3	14.2	dcbpy
Lumo+4	-2.256	1.1	0.7	0.4	11.1	87.4	L_A
Lumo+5	-1.896	2.2	1.9	0.3	4.5	93.0	L_A

Table 5: Molecular orbital composition(%) in the ground state at the B3LYP/LANL2DZ level for **MC**105

Orbital	Energy(eV)	Ru	Ru(d)	NCS	dcbpy	L_A	Main bond Nature
Homo-5	-6.336	61.1	60.8	20.7	8.7	9.5	Ru (d) + SCN
Homo-4	-5.978	15.0	14.9	4.2	2.7	78.1	L_A
Homo-3	-5.054	1.6	1.2	92.3	1.9	4.2	SCN
Homo-2	-4.961	16.0	15.9	75.7	4.1	4.3	SCN
Homo-1	-4.883	12.4	12.2	78.1	6.1	3.5	SCN
Homo	-4.746	21.1	20.8	67.0	7.5	4.4	SCN + Ru(d)
Lumo	-3.245	10.8	10.8	2.5	83.1	3.5	dcbpy
Lumo+1	-2.977	4.5	4.5	0.8	6.7	88.0	L_A
Lumo+2	-2.810	3.3	3.2	0.4	90.9	5.4	dcbpy
Lumo+3	-2.495	1.3	1.2	0.4	4.7	93.5	L_A
Lumo+4	-2.358	0.6	0.2	0.3	91.2	7.9	dcbpy
Lumo+5	-1.895	2.3	1.8	0.3	4.7	92.7	L_A

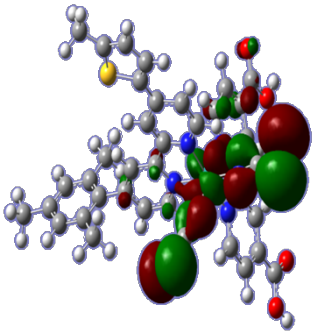

HOMO

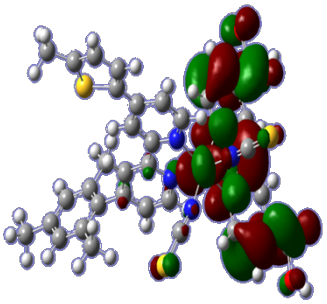

LUMO

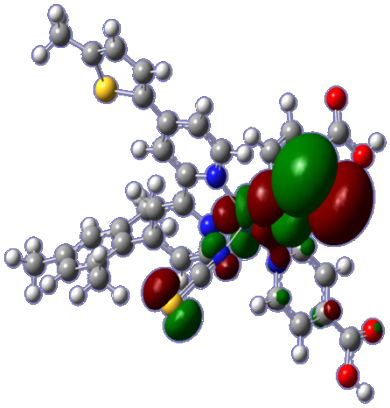

HOMO-1

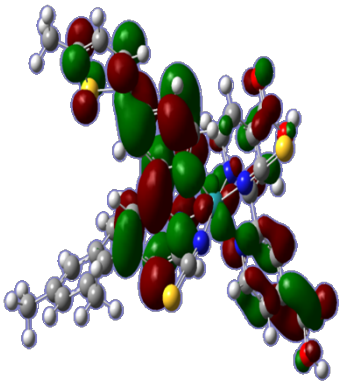

LUMO+1

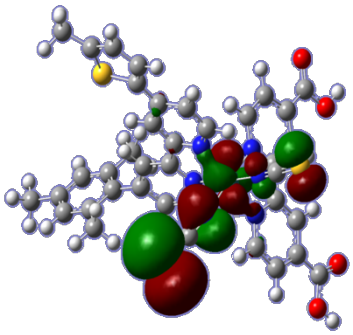

HOMO-2

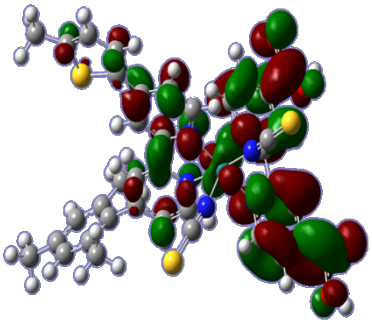

LUMO+2

Figure S29. Isodensity surface plots of frontier orbitals of **MC**103 obtained from DFT calculations.

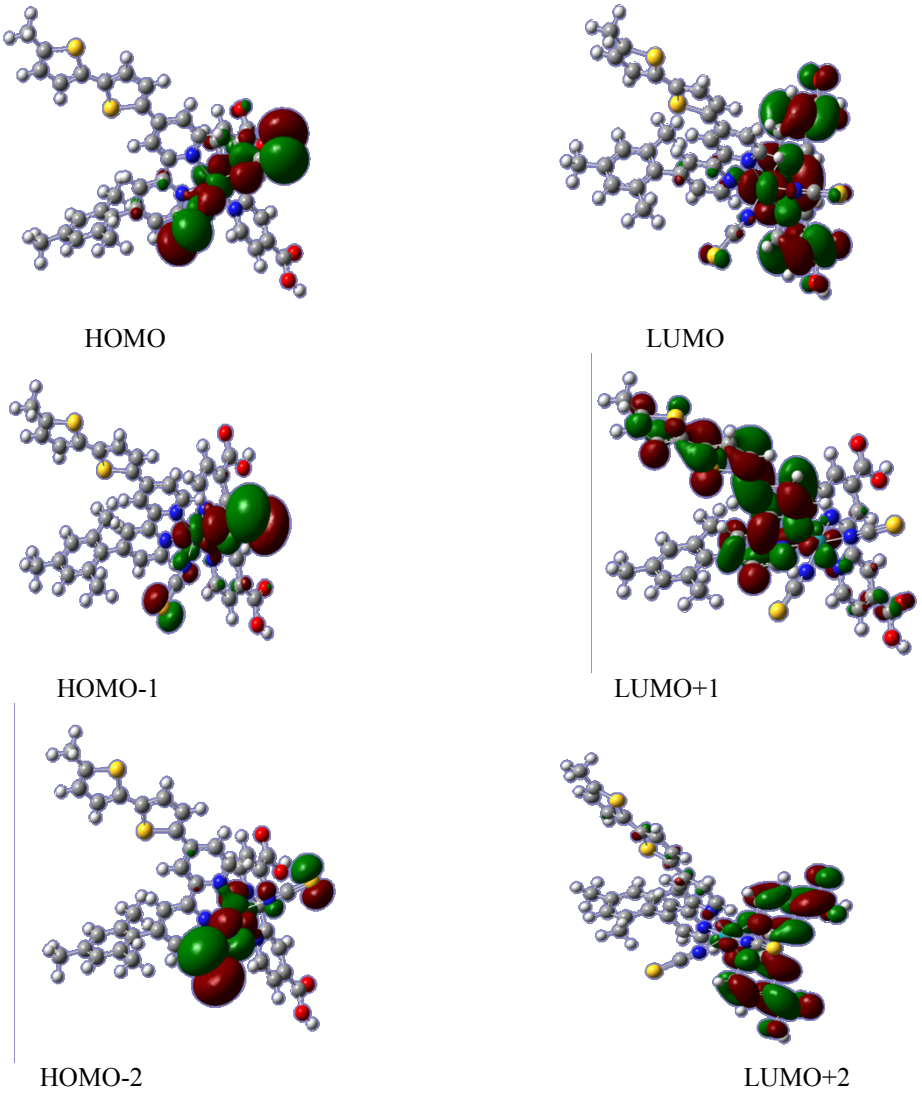

Figure S30. Isodensity surface plots of frontier orbitals of **MC**105 obtained from DFT calculations.